(12) LEVEL III

CHARACTERIZATION AND ANALYSIS OF INDIUM-DOPED SILICON EXTRINSIC DETECTOR MATERIAL

J. Baukus
Hughes Research Laboratories
3011 Malibu Canyon Road
Malibu, CA 90265

T. McGill
California Institute of Technology
Pasadena, CA 91125

L. Forbes
University of California (Davis)
Davis, CA 95616

November 1978

70
DAAK–77–C–0082

Interim Technical Report 2

For period 1 October 1977 to 30 June 1978

Approved for public release; distribution unlimited.

Sponsored by

DEFENSE ADVANCED RESEARCH PROJECTS AGENCY (DoD)

ARPA Order No. 3211, Amendment 3

Monitored by

Philip R. Boyd, NVL

ATTN: DRSEL–NV–FIR

Fort Belvoir, VA 22060

The views and conclusions contained in this document are those of the authors and should not be interpreted as necessarily representing the official policies, either expressed or implied, of the Defense Advanced Research Projects Agency or the U.S. government.

ARPA Order Number	3211, Amendment 3
Name of Contractor	Hughes Aircraft Company
Contract Number	DAAK70-77-C-0082
Effective Date of Contract	31 March 1977
Expiration Date of Contract	30 June 1979
Reporting Period	1 October 1977 through 30 June 1978
Principal Investigator and Phone Number	Dr. Robert Baron (213) 456-6411, Ext. 392
Project Scientist or Engineer and Phone Number	Dr. James Baukus (213) 456-6411, Ext. 204
Short Title of Work	SIMDEC (Silicon Indium Material and Detector Characterization)

UNCLASSIFIED

SECURITY CLASSIFICATION OF THIS PAGE (When Data Entered)

REPORT DOCUMENTATION PAGE

READ INSTRUCTIONS BEFORE COMPLETING FORM

1. REPORT NUMBER

2. GOVT ACCESSION NO.

3. RECIPIENT'S CATALOG NUMBER

4. TITLE (and Subtitle)

CHARACTERIZATION AND ANALYSIS OF INDIUM-DOPED SILICON EXTRINSIC DETECTOR MATERIAL

5. TYPE OF REPORT & PERIOD COVERED

Interim Report, 2
1 Oct 1977 - 30 June 1978

6. PERFORMING ORG. REPORT NUMBER

7. AUTHOR(s)

J. Baukus, T. McGill, and L. Forbes

8. CONTRACT OR GRANT NUMBER(s)

DAAK70-77-C-0082, ARPA Order-3211

9. PERFORMING ORGANIZATION NAME AND ADDRESS

Hughes Research Laboratories
3011 Malibu Canyon Road
Malibu, CA 90265

Robert Barnes

10. PROGRAM ELEMENT, PROJECT, TASK AREA & WORK UNIT NUMBERS

11. CONTROLLING OFFICE NAME AND ADDRESS

Defense Advanced Research Projects Agency
Arlington, VA 22200

12. REPORT DATE

November 1978

13. NUMBER OF PAGES

48

14. MONITORING AGENCY NAME & ADDRESS(if different from Controlling Office)

Night Vision Laboratory
Ft. Belvoir, VA 22060

15. SECURITY CLASS. (of this report)

UNCLASSIFIED

15a. DECLASSIFICATION DOWNGRADING SCHEDULE

16. DISTRIBUTION STATEMENT (of this Report)

Approved for public release; distribution unlimited.

DDC
RECEIVED
DEC 27 1978
B

17. DISTRIBUTION STATEMENT (of the abstract entered in Block 20, if different from Report)

18. SUPPLEMENTARY NOTES

78 12 18 074

19. KEY WORDS (Continue on reverse side if necessary and identify by block number)

Extrinsic silicon, Infrared detectors, SIMDEC program, Photoluminescence, Excitons, IRFET, Capture cross section

20. ABSTRACT (Continue on reverse side if necessary and identify by block number)

This second six-month report of a two-year program describes progress made in analyzing Si:In detector material. Hall-effect, photoluminescence, and IRFET measurements were performed to characterize the X level and to attempt to determine its nature.

DD FORM 1 JAN 73 1473 EDITION OF 1 NOV 65 IS OBSOLETE

UNCLASSIFIED

SECURITY CLASSIFICATION OF THIS PAGE (When Data Entered)

112 690

TABLE OF CONTENTS

LIST OF ILLUSTRATIONS

LIST OF TABLES

SECTION 1

INTRODUCTION

The objective of the silicon indium material and detector characterization (SIMDEC) program being conducted by Hughes under contract DAAK70-77-C-0082 is to investigate the nature of defects in indium-doped silicon detector material and to develop techniques for the control of quality in the growth of extrinsic and high-purity undoped silicon for infrared (IR) detector monolitic chips. The discovery of a second, shallower acceptor level in Si:In, the so-called X level, demonstrated the need for further research on indium-doped silicon. The X level has been observed in measurements of Hall effect versus temperature and of IR photoconductivity and absorption. It is undesirable in extrinsic Si:In photoconductors because its shallower energy level results in excess thermally ionized carriers. These lower the maximum temperature at which background-limited detectivities can be obtained. This can reduce the operating temperature by as much as 10 K with a corresponding increase in cooling power requirements.

The X level has an ionization energy of 0.11 eV and has a concentration that is a direct function of the concentration of the indium. Different growth conditions can produce drastically different amounts of X level in comparably indium doped material samples. Thus, it cannot be a discrete dopant. These facts indicate that the X level is likely to be a complex of indium and some other crystalline defect or impurity. However, the exact physical nature of the X level is unknown, as are the growth and processing factors that determine its concentration. The purpose, then, of the SIMDEC program is to apply the appropriate physical measurements to Si:In to identify the nature of the X level and means of controlling it.

The prime contractor for this program is Hughes Research Laboratories (HRL); the California Institute of Technology (CIT) and the University of California at Davis (UCD) are the subcontractors.

The most significant result during this reporting period is the discovery of a correlation between the X-level concentration and the concentration of carbon. This relationship was determined from X-level data (taken by Hall-effect measurements) and C data (from IR transmission studies). This C dependence explains the higher than expected X-level concentrations observed in float-zone samples, which were found to have C concentrations higher than expected. It also explains the lower X-level values in samples from the large Czochralski grower, which were found to have low C.

Although these results must be considered preliminary pending data on more crystals, a model for the X level can be proposed. The X level may be an In-C pair occupying adjacent substitutional sites in the lattice. The lower X-level concentrations observed after 850°C anneals (as compared with 650°C anneals) are consistent with this model if a reasonable In-C pair binding energy is assumed. There will be fewer In-C pairs in thermal equilibrium at 850°C than at 650°C because of the higher lattice thermal energy. This concentration of pairs is "frozen" by the quench following anneal. A subsequent anneal at 650°C will increase the number of pairs, which is consistent with the observed higher X-level concentration at this anneal temperature. It is not necessary to invoke Yoshihiro's[1] observation of a minimum in substitutional carbon at 800°C, which in fact we do not see with our much shorter anneals.

The source of the carbon in the Czochralski-grown Si:In is probably the graphite heaters used to melt the poly-silicon. Since the heater is not used at full power in the large Czochralski grower, less C is likely to be vaporized from it during growth. Since a causal relationship between C and the X level has been found, it now becomes possible to consider ways to modify the Czochralski growers to minimize the X-level concentration and eliminate this problem for Si:In photoconductive detectors.

The results of studies carried out at HRL are contained in Section 2. Two additional crystals were grown for the program during this period, and the results of Hall-effect analysis are presented and compared with the predicted dopant profiles. IR transmission data and the concentrations of indium, oxygen, and carbon obtained are discussed. Also discussed are the Hall-effect evaluations of material processed at UCD.

An intentionally uncompensated crystal was found to contain an excessive amount of boron; the origin of the boron is presently being investigated. The second crystal was a simulation of Si:In crystals pulled at Hughes Industrial Products Division, Carlsbad, California (IPD). Since this crystal contained a high X-level concentration, several growth parameters (e.g., argon overpressure, melt surface area to volume ratio, crucible material, and silicon starting material) were eliminated as potential causes of the X level. The spectroscopic studies indicated that the X level is uncorrelated to the oxygen concentration but is strongly correlated to the carbon concentration in the crystal. Several changes were observed in the material processed at UCD, indicating that dopant concentrations obtained on the original ingot should not be relied on when making device calculations.

The progress at CIT during this period is described in Section 3. The three strongest photoluminescence lines observed uniquely in Si:In were investigated. The temperature and time dependencies of these line strengths were measured. The results indicate that these lines are due to an isoelectronic trap (or traps) and not to an acceptor, such as the X level.

Characterizations of deep level impurity center concentrations, energy levels, thermal and optical emission rates, and thermal capture cross sections were performed by UCD during this reporting period using the MOSFET structure. Indium concentrations measured by several methods (variation of the MOSFET threshold voltage with substrate bias, reverse bias junction capacitance, and resistivity versus temperature) were found to be typically a factor of two less than results from Hall-effect measurements. The indium hole emission rate at 77 K was found to be 6.0 msec

with a 0.15 eV activation energy for a lightly doped sample and 20 μsec and 0.117 eV for a more heavily doped sample. The hole capture coefficient was found to be 3.7×10^{-7} cm^3/sec. Small transients in the thermal emission rate, associated with the X level, were observed, which indicate a capture coefficient of 1.5×10^{-6} cm^3/sec at 35 K for this level. Measurements of Si:In photoconductors are also included. The description of this work will be published later.

The appendices to this report contain reprints of papers given at the 1978 IRIS Detector Specialties Group Meeting.

SECTION 2

CRYSTAL GROWTH AND CHARACTERIZATION

This section describes progress at HRL during this reporting period. The growth and analysis of two additional crystals are discussed. An evaluation program to characterize silicon in terms of its oxygen and carbon content using IR spectroscopy is described, and the initial results are presented. Results of Hall-effect analysis of material processed at UCD are also given.

A. CRYSTAL GROWTH

Ingot C076 was grown in a 1-kg system as part of the SIMDEC program to produce a very lightly counterdoped crystal with a low boron concentration. The principal sources of boron in Czochralski-grown silicon are the starting polycrystalline silicon and the quartz crucible, which dissolves slowly in the melt during growth and releases its boron impurity. Low boron starting material was used and the growth was from a Suprasil-lined crucible. This type of container was used because Suprasil has a significantly lower boron content than does regular quartz, which is typically used for crucibles. Since B cannot be removed from Si during the growth process to any significant extent, care must be taken to minimize its introduction during growth. Although Suprasil has a higher dissolution rate into Si, the B buildup in the melt is considerably slower than for regular quartz. This results in a crystal with lower B concentration.

Since P must be added to compensate for the B, crystals grown with this type of crucible require less P to be added to ensure that $N_P > N_B$ throughout the ingot. Therefore, they will have a lower net compensation and a corresponding higher detector responsivity. Since the values of N_P and N_B are lower, their difference can also be kept smaller.

No P was intentionally added during the growth of crystal C076. The major sources of P were the silicon starting material, which had an initial P concentration of 8×10^{12} cm^{-3}, and the crucible. Phosphorus

tends to build up in the melt (and the crystal) during growth because its segregation coefficient is less than one. The rate of this buildup is reduced by evaporation of P from the melt under the low-pressure condition of the crystal growth. The overall result under these conditions is a net increase in B relative to P in the crystal from seed to tang due to the rate of B buildup from crucible dissolution.

Table 1 lists the results of Hall-effect versus temperature measurements on three samples from ingot C076. The samples labeled "A" are from the seed end of the crystal. The "M" sample is from about midway between the seed and tang. All samples are from the center of the wafer from which they were cut. Sample A20 received a 650°C anneal for 30 min to reduce the oxygen donor content. Samples A30 and M30 received an 850°C anneal for 60 min, which we have found reduces the X-level concentration and the oxygen-donor concentration.

The 850°C anneal reduced the X level as can be seen by comparing samples A20 and A30. In addition, the X level increases in the crystal from seed to tang. Samples A20 and A30, which were adjacent, differ by an order of magnitude in net compensation, N_D-N_B. This is apparently due to slight fluctuations in an extremely close balance between the P and B concentrations. Both B and P increased in concentration toward the center, axially, of the ingot; B increased more rapidly, as expected.

Table 1. Dopant Concentrations in Crystal C076

	A20	A30	M30
N_{In}, 10^{17} cm^{-3}	1.4	1.3	1.8
N_X, 10^{13} cm^{-3}	62-170	5.7	45
N_B, 10^{13} cm^{-3}			15
N_D, 10^{13} cm^{-3}			5.3
N_D-N_B, 10^{13} cm^{-3}	0.18	1.4	

6303

An analysis of the pickup of B and P in crystal C076 was made using a model developed by H. Kimura.[2] The dopant concentrations measured on the Hall samples were used as boundary conditions, and initial values of B and P in the melt were calculated to be 1.7×10^{14} B/cm^3 and 8×10^{14} P/cm^3. This amount of B far exceeds the amount possible due to crucible dissolution. However, it corresponds to 0.6 ppm in the indium material used for doping. This is within the manufacturer's specification for purity of 6-9's indium. Other Si:In crystals doped with this material were also doped with P and were grown in regular quartz crucibles; as a result, this amount of B pickup would not be observed.

The results of measurements of crystal C076 suggested several experiments, which are now underway. A section of this crystal is undergoing several passes of vacuum float zoning to remove the In and P, leaving only the B in its original distribution. This will allow a verification of the model on which the calculations were based. Another crystal is being grown using In obtained from IPD. This material is known to have a lower B concentration. The In dopant material currently being used will be baked under a controlled atmosphere to reduce its B content. Samples of In from HRL and IPD will be analyzed for impurities by mass spectroscopic techniques.

Crystal C055 was an experiment to simulate, using a small (1 kg) grower at HRL, growth of Si:In crystals in the large crystal grower at IPD. The same polysilicon starting material and In and P dopant materials were used, and the gas overpressure and the pull and rotation rates were the same. The ratio of crystal diameter to crucible diameter was also identical. The object of this simulation was to determine if any of these growth parameters influenced the X level. The results of Hall-effect measurements of samples from the center of the seed end of this ingot are presented in Table 2. Sample A30 had a 650°C anneal for 30 min, and sample A40 had an 850°C anneal for 1 hr. The ingot has a rather high X-level concentration, one similar to the levels observed in crystals grown under the normal conditions for this machine. Since this crystal was grown under the same conditions as crystals at IPD that consistently exhibit X-level concentrations at or below 10^{14} cm^{-3}, it is unlikely that these growth parameters are influencing the X level.

Table 2. Hall-Effect Results for the Seed End of Crystal C055

	A30	A40
N_{In}, 10^{17} cm^{-3}	1.6	1.8
N_X, 10^{14} cm^{-3}	30	5.8
$N_D - N_B$, 10^{14} cm^{-3}	2.7	2.4

6303

B. IR SPECTROSCOPIC STUDIES

IR measurements of Si:In grown under different conditions and with varying In doping levels were begun during this reporting period to determine the oxygen and carbon content of the crystals and the relationship, if any, of these impurities to the X-level concentration. A correlation between In concentration and X-level concentration has been reported[3-5] and substantiated by others.[6-8] However, since samples grown under different conditions with similar In concentrations show differences in the X-level concentration, it is unlikely that the X level is a simple In complex. At least one more component appears to be necessary.

The experimental apparatus consisted of two liquid-nitrogen dewars designed and fabricated at HRL; the dewars are compact enough to fit into the sample and reference compartments of the Beckman IR-12 IR spectrometer. The double-beam-difference method was used to obtain the absorption spectrum of the sample. An oxygen- and carbon-free sample of undoped, zone-refined Si (furnished by John Baker, Dow Corning) was mounted in the reference dewar, and the sample to be tested was mounted in the matching dewar in the sample beam. Both dewars have CsI windows that allow measurements to be made to 30 μm. The double-beam-difference method canceled the lattice absorptions that appear near both the oxygen and carbon impurity center peaks. Because of the lattice absorption interference, care was taken to assure that both the unknown and the

reference samples were of the same thickness. (This measurement technique and others are described in Refs. 9 and 10.) There has traditionally been disagreement among experimenters as to the correct calibration factor to use to convert optical data to oxygen and carbon concentrations.[11] The relationships used in this study between the peak absorption coefficients at liquid nitrogen temperature (α_O and α_C) and concentrations (atoms/cm^3) are

$$[O] = 1.43 \times 10^{17} \alpha_O$$

$$[C] = 3.1 \times 10^{16} \alpha_C \quad .$$

The oxygen calibration is derived from Refs. 9 and 10 scaled to 77 K, and the carbon calibration is from ASTM F123-74 corrected for a different baseline. The limits of sensitivity for measuring oxygen and carbon concentrations are 1×10^{15} atoms/cm^3 and 2×10^{15} atoms/cm^3, respectively.

The results obtained to date are given in Table 3. Additional optical and Hall-effect measurements are in progress on these and other samples. Figure 1 shows X-level concentration normalized by the In concentration (both obtained from Hall measurements) plotted against the interstitial oxygen concentration obtained from the optical measurements. The circles are HRL measurements and are labeled with the crystal number. The triangles are data from solution-grown Si:In crystals grown and measured at Honeywell.[12] Clearly, no correlation exists with the oxygen concentration. Sample Z008 is particularly significant in this regard as it has at least three orders of magnitude less oxygen and yet is comparable to the other samples in X level.

In contrast to the lack of correlation seen for the X level and oxygen concentrations, Figures 2 and 3 show a definite correlation to carbon concentration. In Figure 2, the X-level concentration normalized to the In concentration is plotted versus the carbon impurity concentration. In Figure 3, the X-level concentration is plotted against the carbon concentration.

Table 3. Summary of Hall-Effect and IR Transmission Measurements

Sample	N_{In}, 10^{17} cm^{-3}	N_X, 10^{14} cm^{-3}	N_X/N_{In}, 10^{-3}	α_{In}, cm^{-1}	σ_{In}, 10^{-16} cm^2	N_O, 10^{17} cm^{-3}	N_C, 10^{16} cm^{-3}
C008.T	2.6	32	12			14.3	6.0
C014.1	1.2	4.7	3.9	9.63	0.80	14	1.9
C014.3	1.5	22	15	14.7	0.98	13	30
C20102	0.60	5.2	8.7	6.6	1.1	9.6	3.0
C71601.3	1.3	1.1	0.85	8.4	0.65	7.4	0.56
Z008	1.3 - 2.4	1.8 - 8.5	1.3 - 4.3	10.2	0.42 - 0.78	<0.01	2.11
C076	1.4	6.2 - 17	4.5 - 12			6.9	2.8

6303

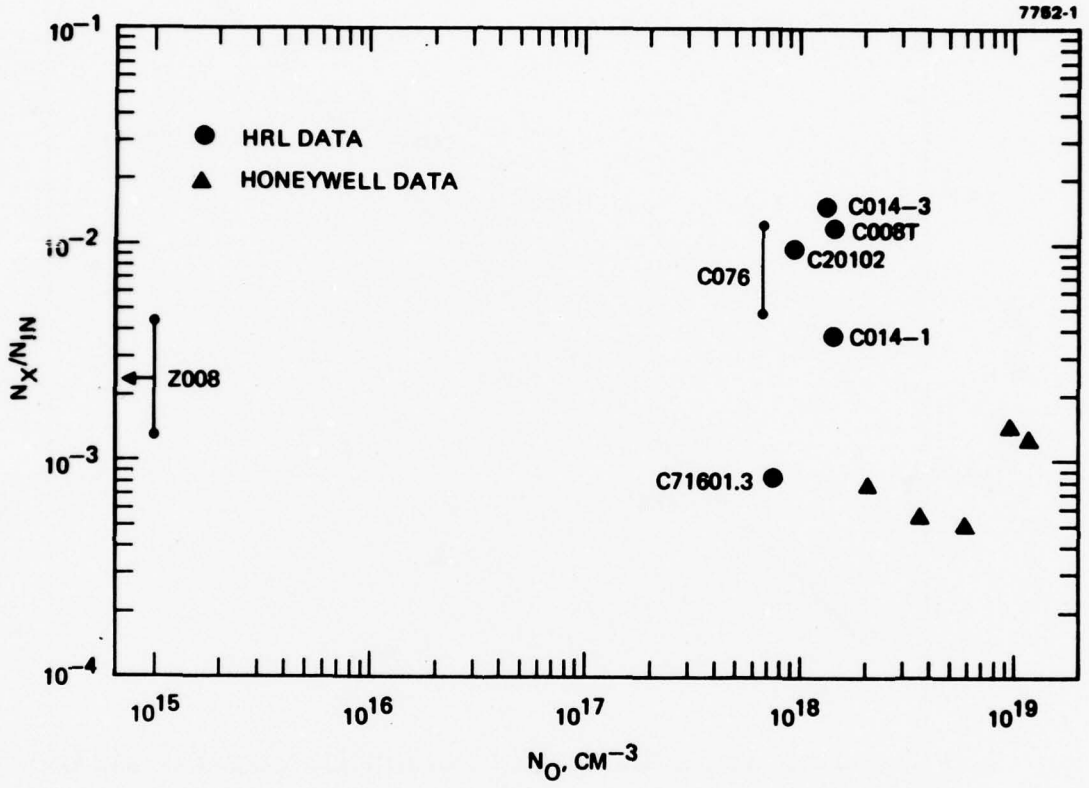

Figure 1. The ratio of X-level concentration to indium concentration versus the oxygen concentration.

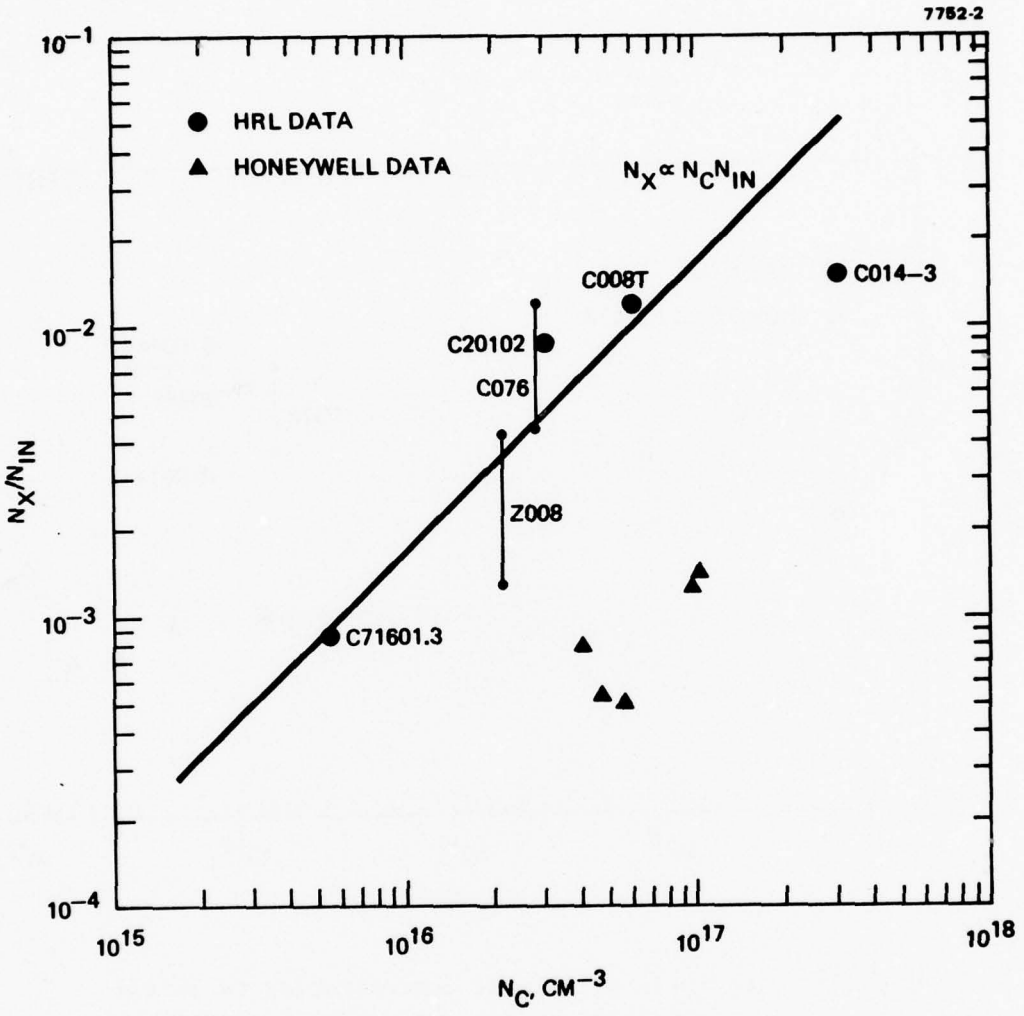

Figure 2. The ratio of X-level concentration to indium concentration versus the carbon concentration.

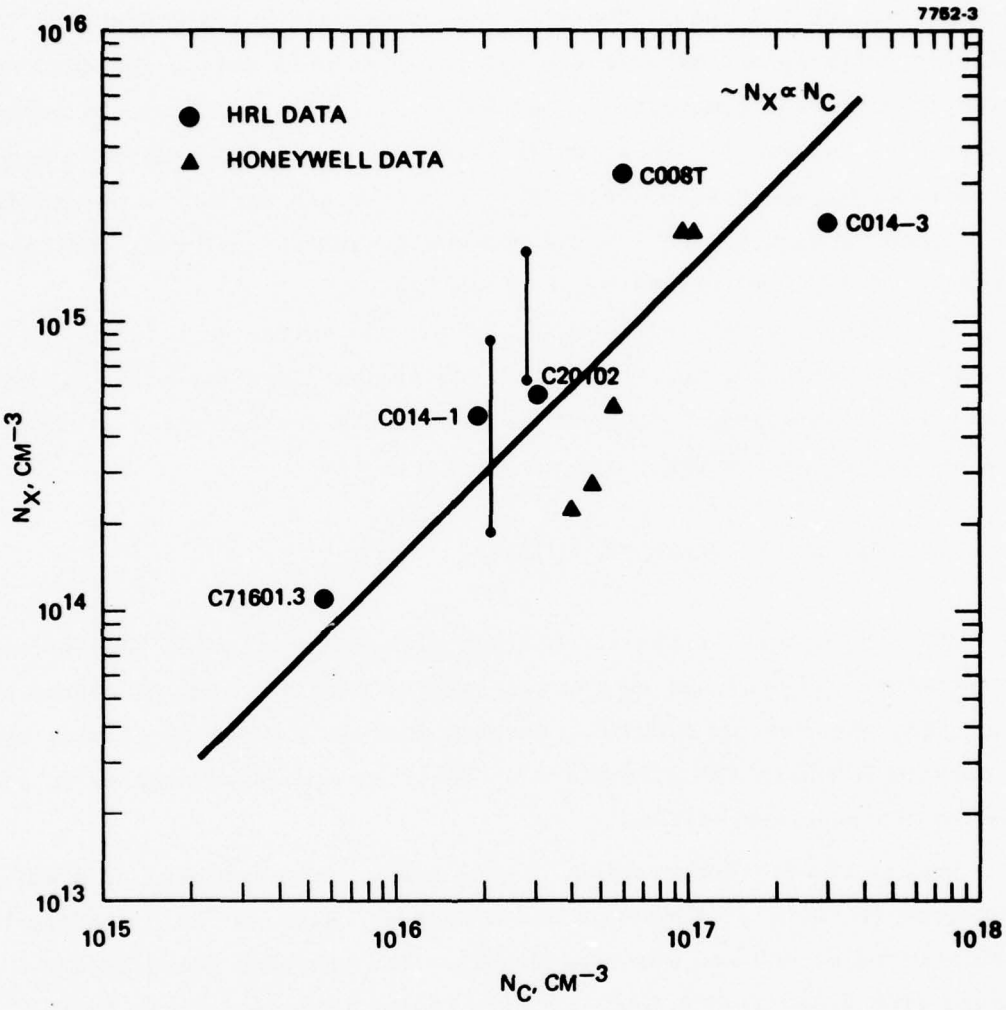

Figure 3. The X-level concentration versus the carbon concentration.

The vertical lines for samples Z008 and C076 represent the uncertainty in X-level concentration for these samples. This uncertainty occurs because the optical and Hall-effect crystals were not from the same portion of the ingot. There is also uncertainty concerning the relative calibrations between the HRL and Honeywell data. The data were taken at different temperatures and only absorption coefficients were reported by Honeywell. Thus, while relationships to the carbon concentration can be ascertained, relative concentrations cannot be obtained. The carbon concentrations for the Honeywell samples represent our best estimate of the appropriate calibration factor.

It appears that the ratio N_X/N_{In} gives the better correlation to the carbon concentration, but there are insufficient data for a conclusive result to be obtained. Other samples currently are being measured; these samples represent a wider range of the parameters.

C. ANALYSIS OF UCD-PROCESSED MATERIAL

HRL, in support of its subcontract with UCD, performed Hall-effect measurements and analyses on several samples that had been processed at UCD. This was done to correlate measurements at the two facilities and to provide UCD with the parameters of their as-processed samples in addition to the as-grown values.

During the previous period, a Hall sample from the edge of a wafer processed at UCD was fabricated and measured. Also, a "bulk resistor" manufactured at UCD was measured at HRL. The resistor measurements agreed with those at UCD, but not with resistivity data taken on the Hall sample from the same processed wafer. During the present period, the actual device was fabricated into a Hall sample and measured. The results are shown in Figure 4, which is a plot of resistance versus temperature. The solid line and discrete points are the bulk resistor measurements of HRL and UCD, respectively. The dashed line is from the edge of the UCD-processed wafer, and the dash-dotted line is from the Hall sample made from the bulk resistor. The last two curves were

obtained by multiplying the measured resistivity data by 18, which is the ratio of resistance to resistivity of these devices calculated by UCD. The bulk resistor gives a good measure of the substrate resistivity, except at the higher temperatures. This error is apparently due to contact resistance in the bulk resistor.

Figure 4 indicates a significant difference between the center and edge samples from this wafer. This effect is also seen in the dopant data from Hall-effect measurements, which is given in Table 4. Sample C010LF.10A is the Hall sample from the bulk resistor, and sample C010LF.410 is from the edge of the same processed wafer in a diffusion-free region. The indium concentration is not significantly different in the two samples, but the X level is dramatically lower and the net donor concentration is also lower. This result is not consistent with data from unprocessed wafers, which do not show large variations from center to edge.

Table 4 also contains data from the edge of another UCD-processed wafer, D, from crystal C010 and the data from seed and tang of the original ingot. This sample showed an increase in net donor concentration after processing. Data from the edge of a UCD-processed wafer from crystal C042 and the original seed and tang data are included in the table. The processed edge sample again shows an increase in net donor concentration. In this case, the X level also increased slightly. The specific cause of these processing effects is unknown, and their investigation is beyond the scope of this program.

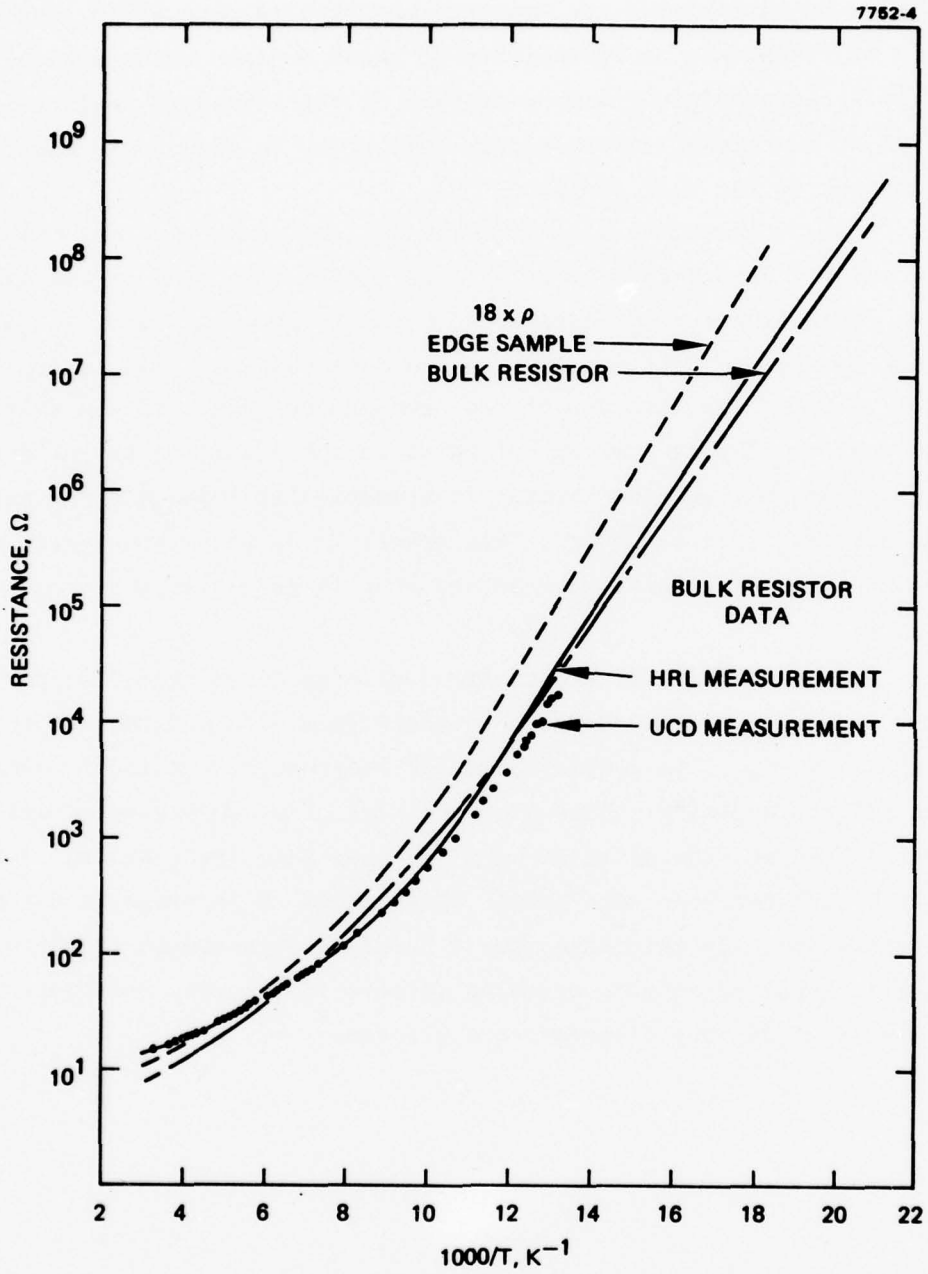

Figure 4. Various measurements of the resistance of the UCD "bulk resistor."

Table 4. Dopant Concentrations of UCD-Processed Material

Sample	N_{IN}, 10^{15} cm^{-3}	N_X, 10^{14} cm^{-3}	N_D-N_B, 10^{14} cm^{-3}
C010LF.D10 Run 13 Edge	1.3	3.4	3.7
C010LF.10A Run 4 No. 10	2.0	0.37	0.15
C010LF.410 Run 4 Edge	2.2	10	0.47
C010 Seed-Tang	0.95-4.0	7.6-29	0.86-0.44
C042LF.10A Proc. Edge	2.3	1.0	1.4
C042 Seed-Tang	1.9-2.3	0.29-0.32	0.67-0.67

6303

SECTION 3

PHOTOLUMINESCENCE STUDIES IN EXTRINSIC SILICON

This section, which describes the work done at CIT during this reporting period, was written by Prof. Thomas McGill.

The primary aim of the work has been to explore the origin of several lines observed in Si:In. The three strongest of these lines, at 1108.6, 1115.9, and 1117.7 meV, have been studied in detail. In particular, the temperature dependence and the time dependence of these lines have been measured.

A. SPECTRUM OF Si:In

Figure 5 gives a spectrum for a Si:In sample grown by the Czochralski method. The spectrum shows not only the now well established bound exciton (BE) lines, but also several lines of unknown origin.

B. DECAY MEASUREMENTS ON THE A, B, C LINES

The decay transients of the A, B, C lines have been measured as a function of temperature. Typical results for 15 K are shown in Figure 6. The most striking aspect of these decay transients is the very large value for the decay time, several hundred microseconds. These times should be compared with those obtained for other lines. For example, the decay time for free excitons in the purest Si available is about 2.6 μsec,[13] and the decay time for excitons bound to neutral impurities is less than a few μsec.[14] Hence, the decay times of A and B are approximately two orders of magnitude larger than the decay times usually observed with this measurement technique.

These very long decay times suggest that the center that is binding the exciton does not contain a free carrier. For if the center did contain a free carrier, the Auger decay rate involving the ionization of this

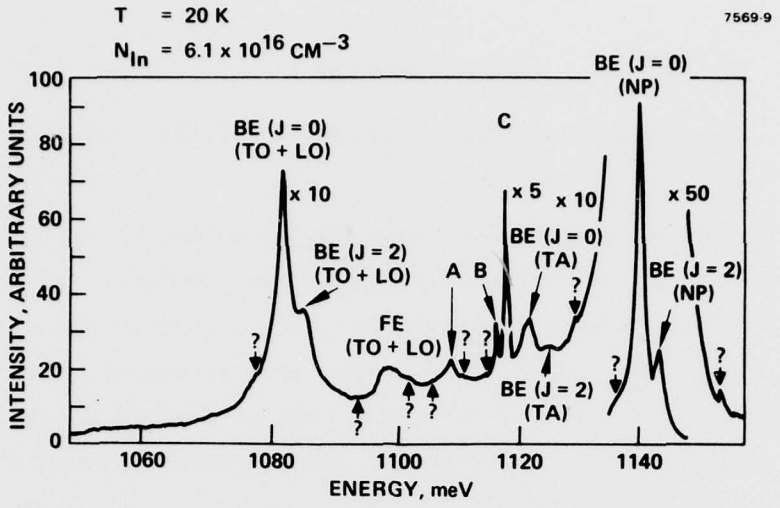

Figure 5.
The luminescence from a Czochralski-grown Si:In sample. The lines labeled BE are due to an electron-hole pair bound to a neutral In. The lines labeled with A, B, C, and ? are of unknown origin.

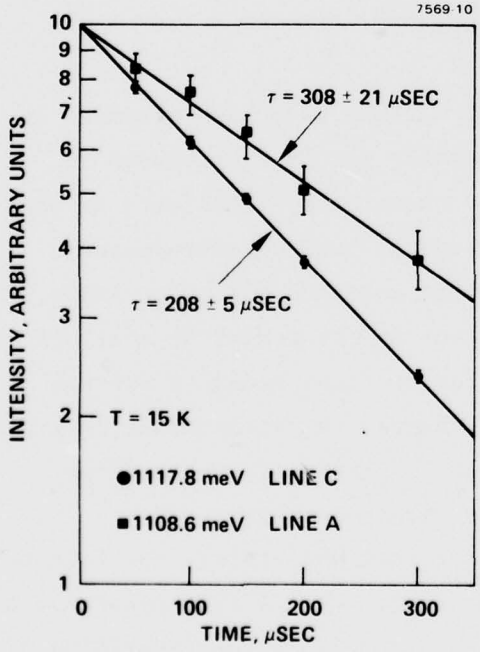

Figure 6.
The decay characteristics of the lines labeled A and C in Figure 5.

center would be many orders of magnitude faster than the observed decay rate. Hence, these lines might be interpreted as resulting from excitons bound to isoelectronic traps. Since these lines have only been observed in samples doped with In, this isoelectronic trap is expected to be a complex involving perhaps an In and some other species (e.g., vacancy, O, N, C). These lines are the first published results on the decay of isoelectronic centers in Si.

C. TEMPERATURE DEPENDENCE

To examine the question of whether any one of the lines A, B, or C involves different states of excitons bound to a center, we measured the temperature dependence of the ratio of the intensities of these lines. If two of the lines result from different initial states of the same center, then the ratio should vary as

$$e^{-\Delta E/kT} ,$$

where ΔE is the splitting between these lines. The variation of these ratios is plotted in Figure 7. The fact that none of these ratios has the expected dependence indicates that they do not result from different initial states on the same center. The data show that the ratio of A to B is independent of temperature, which might suggest that these lines occur because of different final states of the impurity. However, since the A and B lines have different decay times, they do not occur because of transitions resulting from the same initial state going to different final states.

The results of measurements of the temperature dependence of the decay times are given in Figure 8. These data show a temperature dependence that is at least partially understood. If, at high temperatures, a carrier or an exciton is released from the center, this would explain the observed decrease in the decay time. Plots of the high-temperature data versus inverse temperatures yield values of the ionization energy of 29.4 ± 0.8 meV, 29.5 ± 0.4 meV, and 28.3 ± 0.2 meV for the A, B, C

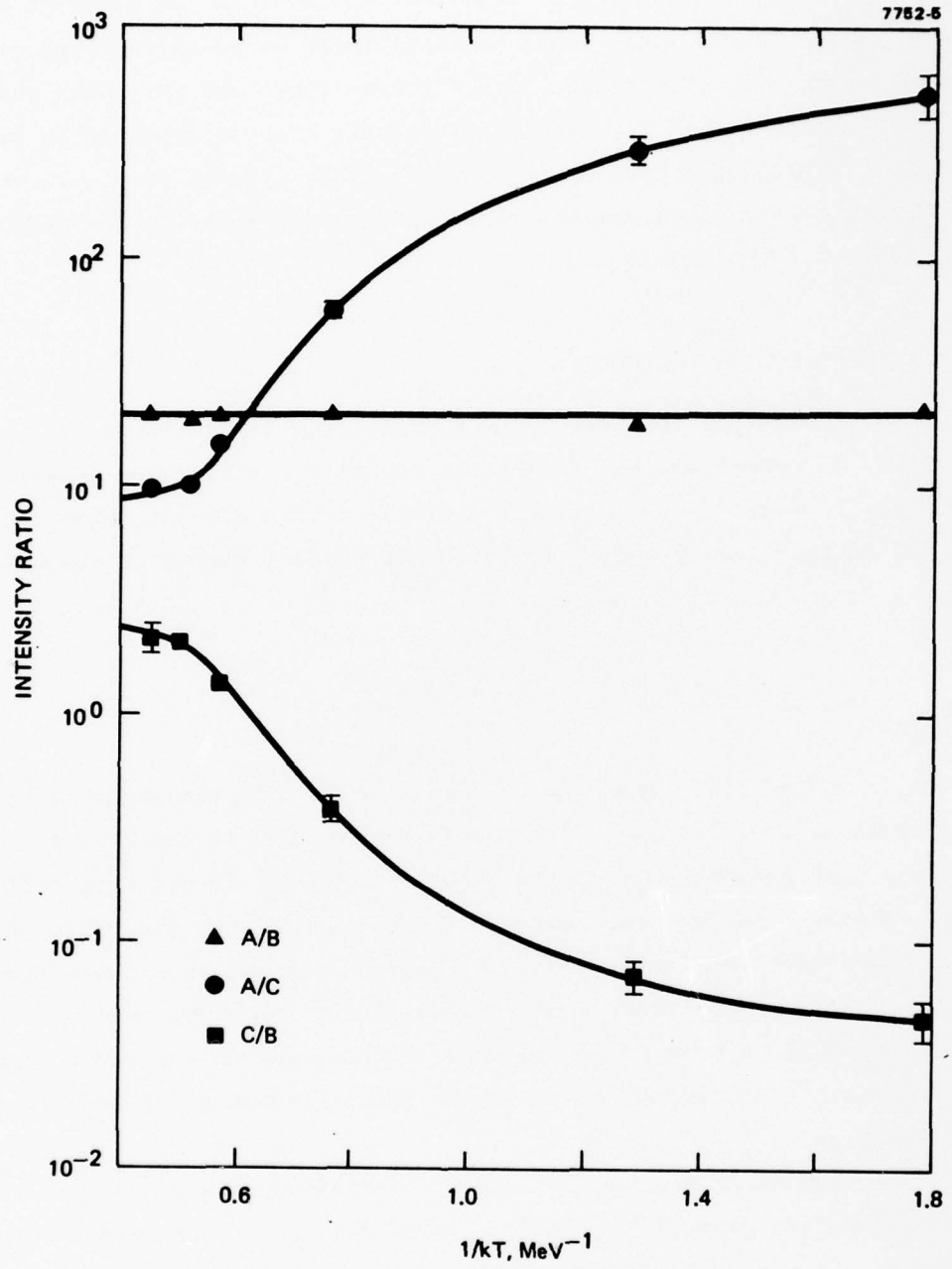

Figure 7. The variation of the intensity ratios of the lines labeled A, B, and C in Figure 5, as a function of temperature.

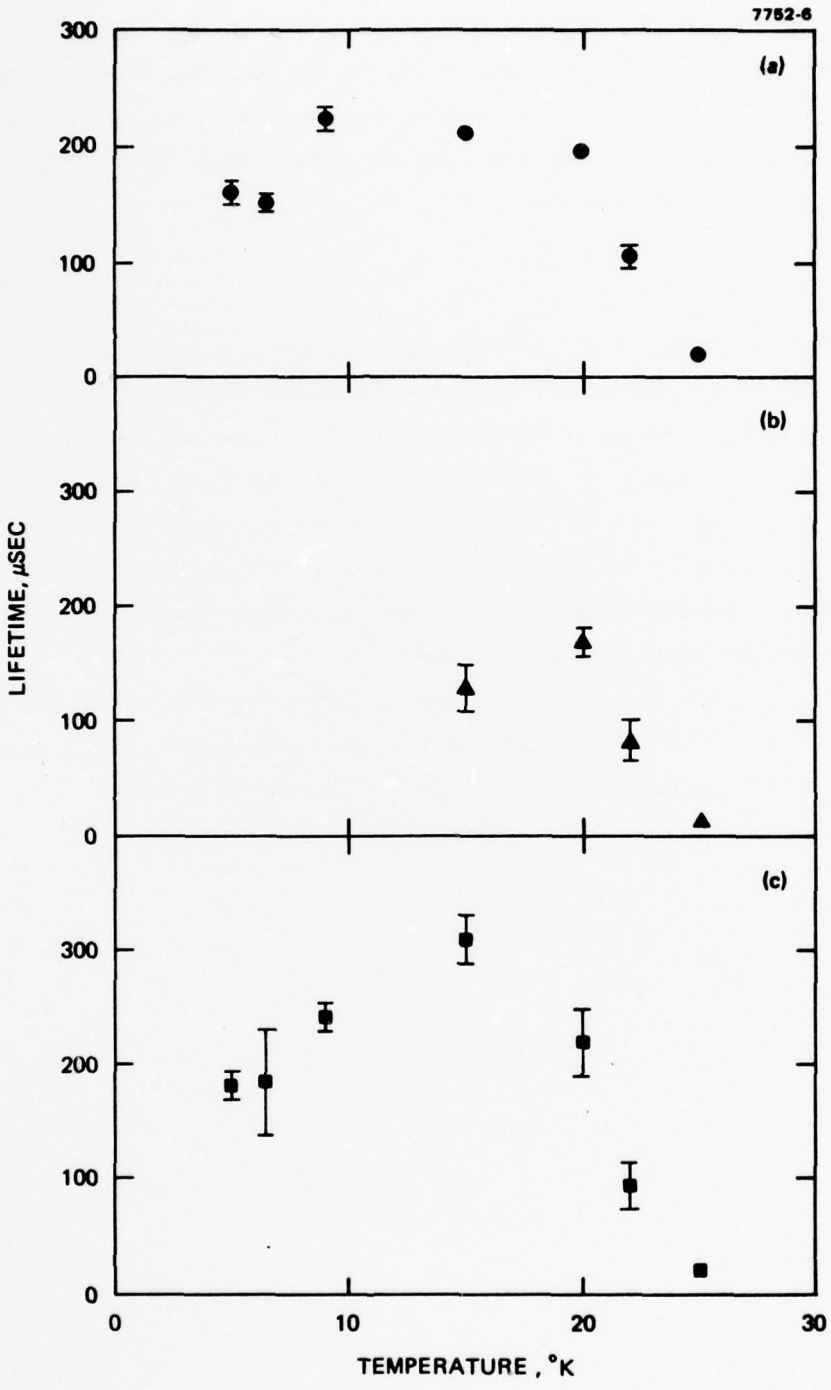

Figure 8. The variation of the decay times of the lines labeled A, B, and C in Figure 5, as a function of temperature.

lines, respectively. These values are about 10 meV smaller than the binding energy of the exciton obtained by assuming that the observed line is due to a non-phonon transition. However, it is possible that the ionization is of a single carrier rather than of the electron and hole into an exciton state.

D. SUMMARY

The observation of the long decay times for the A, B, and C lines indicates that they cannot be directly associated with the X level. The long decay times suggest an isoelectronic center, and we know that the X level is electrically active (i.e., acts as a true acceptor). The small amount of information we have on the relative intensity of these lines with respect to the bound exciton on the In as a function of anneal treatment suggests that they increase in number when the X level increases and decrease when the X level decreases.

The present activity is aimed at exploring the variation of the other lines of unknown origin with anneal treatment. This program is aimed at identifying which line is due to the X level.

SECTION 4

SUMMARY

Progress during this period consisted of efforts aimed at characterizing the Si:In X level. Several measurement techniques were used to search for correlations between the X-level concentration and other crystal defects or growth conditions. These included IR transmission studies to determine oxygen and carbon concentrations and growth studies to determine the effects of gas overpressure; melt surface to volume ratio; and crucible, polysilicon, and doping materials.

Other studies continuing during this period included investigations of new characterization techniques to verify the X-level determinations made by the usual Hall-effect and photoconductive techniques. These new techniques, photoluminescence and MOSFET studies, may lead to new insights into the nature of the X level. For example, a large number of lines are observed in the photoluminescence of Si:In. These lines may contain spectral information about the X level. In addition, these techniques may become useful general analytical tools for semiconductor characterization.

The most significant result during this period was the discovery of a correlation between the X-level concentration and the concentration of carbon. The major thrust of the program will be to confirm this result and to verify that growth in a carbon-free environment will yield low (or zero) X level Si:In.

REFERENCES

1. Kishino, S., Kanamori, M., Yoshiriro, N., and Iizuka, T., Electronic Materials Conference, Santa Barbara, Ca. (1978).

2. CCD-Squared Final Report, Contract DAAH01-75-C-0276, Hughes Aircraft Co. (1978).

3. Baron, R., Young, M.H., Neeland, J.K., and Marsh, O.J., *Appl. Phys. Lett.* 30:594 (1977).

4. Pines, M.Y., and Baron, R., Proc. Int. Electron Dev. Meet., Washington, DC (1974).

5. Baron, R. et al., Proc. IRIS Det. Spec. Group Meet. (1977).

6. Scott, W., *Appl. Phys. Lett.* 32:540 (1978).

7. Scott, W., Proc. IRIS Det. Spec. Group Meet., (1977).

8. Thomas, R.N., Braggins, T.T., Hobgood, H.M., and Takei, W.J., *J. Appl. Phys.* 49:2811 (1978).

9. NBS Technical Note 529.

10. ASTM Bulletin F121-76.

11. Patel, J.R., *Semiconductor Silicon* 1977, edited by H.R. Huff and E. Sirtl (The Electrochemical Society, Princeton, N.J., 1977) p. 521.

12. Studies of Indium-doped Silicon, Semi-Annual Report, 1 Aug. 1977 - 31 Jan. 1978, Contract DAAK-77-C-0194, Honeywell Inc. (1978).

13. Cuthbert, J.D., *Phys. Rev.* B1:1552 (1970). We have measured a lifetime of 1.7 μsec in lightly doped (∿10 Ω-cm) Si.

14. Lyon, S.A., Osbourn, G.C., Smith, D.L., and McGill, T.C., *Solid State Comm.* 23:425 (1977).

. . . . This paper is UNCLASSIFIED

PHOTOCONDUCTIVE PROPERTIES OF INDIUM-DOPED SILICON

J.P. Baukus, R. Baron, M.J. Sheets, and O.J. Marsh
Hughes Research Laboratories
Malibu, California 90265

ABSTRACT

The properties of indium-doped silicon as a material for use as an extrinsic photoconductor was investigated. Detector structures were fabricated from characterized material. Responsivity, D^*, current-voltage characteristics, and spectral photoconductive response were obtained as functions of bias and temperature. Carrier lifetime and recombination coefficient will also be presented as functions of bias, temperature, and donor concentration. The effect of the X level on the maximum operating temperature for various photon backgrounds will be discussed.

1. INTRODUCTION

We are studying Si:In material for use in infrared detectors to determine the suitability of these crystals for monolithic focal plane array (MFPA) applications. Discrete detectors are fabricated and studied to determine material properties and to correlate with Hall-effect data.

The material was grown by both float-zone and Czochralski methods in the <111> and <100> orientations. Two-inch-diameter Czochralski ingots were grown in both large and small melt volume growers. Detectors were cut from areas of wafers adjacent to Hall-effect samples so that accurate comparisons could be made between measurements made on the two types of samples. Detector contacts were formed by ion implantation of boron and by chrome-gold metallization. They were mounted in a variable-temperature dewar that had cold germanium and room-temperature KRS-5 windows. The 300 K background was limited to a 30° field of view by a cold aperture. The signal source for responsivity measurements was a 500 K blackbody chopped at 1000 Hz. The signals and noise were amplified by a room temperature transimpedance amplifier with an adjustable feedback resistor and measured with a tuned voltmeter. Photoconductive spectral responses were taken with a modified Beckman IR-12 spectrometer.

2. RESPONSIVITY

Responsivity, measured as a function of bias voltage and temperature, is plotted in Figure 1 as a function of bias current. This result for Si:In is the same as observed in Si:Ga,[1] that is, the responsivity varies linearly with bias current at temperatures and fields low enough that excess carriers are not generated, either because of thermal ionization or the onset of impact ionization. The departure of the data from the unity slope line at the higher temperatures is a direct measure of the current resulting from thermal ionization; the bias current is the sum of this current and the photocurrent produced by the background. There is a dc component of current produced by the 500 K blackbody, but this contribution is small compared to that resulting from the background.

*This research was supported by the Defense Advanced Research Projects Agency and monitored by the Army Night Vision Laboratory under Contract No. DAAK70-77-C-0082.

[1] J.P. Baukus, M.H. Young, R. Baron, M.J. Sheets, and O.J. Marsh, Proc. IRIS Det. Spec. Group Meet. (1977).

Peak responsivities at 6.4 μm in excess of 50 A/W were measured. The responsivity, normalized to bias field, for this sample and another is plotted in Figure 2 as a function of temperature for a range of biases from 200 to 6500 V/cm. The curves become progressively flatter (the reason is unknown) as the temperature or bias is increased, which reduces the MPFA cooler power requirement.

3. EFFECT OF X LEVEL ON OPERATING TEMPERATURE

The detectivity of an Si:In extrinsic detector is given by

$$D^* = \frac{\lambda}{2hc}\sqrt{\frac{\eta}{Q_B + Q_{TH}}} \quad , \tag{1}$$

where the equivalent thermal background flux is given by

$$Q_{TH} = \frac{\alpha(\eta)\ BN_V}{\sigma_{In} g}\ e^{-\frac{E_{In}}{kT}} \quad . \tag{2}$$

Eq. 2 holds only if In dominates the thermal equilibrium carrier concentration at low temperatures. If the X level dominates this behavior, then Q_{TH} is given by

$$Q_{TH} = \frac{\alpha(\eta)\ BN_V}{\sigma_{In} g}\ \frac{N_X}{N_{IN}}\ e^{-\frac{E_X}{kT}} \quad . \tag{3}$$

If N_X/N_{In} becomes so small that Q_{TH} from Eq. 3 becomes $\lesssim Q_{TH}$ from Eq. 2, then Eq. 3 will no longer be valid, and Eq. 2 should be used. Also, if $N_X \lesssim N_D$, the X level no longer dominates the low-temperature carrier concentration, and a transition is made to Eq. 2, which becomes valid for $N_X << N_D$.

By setting $Q_{TH} = Q_B$, expressions for T_{BLIP} can be derived to yield

$$T_{BLIP} = \frac{E_{In}/k}{\left[\ln \frac{\alpha(\eta) BN_V}{\sigma_{In} g Q_B}\right]} \tag{4}$$

if Eq. 2 is valid and

$$T_{BLIP} = \frac{E_X/k}{\left[\ln \frac{\alpha(\eta) BN_V N_X}{\sigma_{In} g Q_B N_{In}}\right]} \tag{5}$$

if Eq. 3 is valid.

To test the agreement of the data with the theory, it is convenient to plot $\ln[(\alpha(\eta)\ N_V/QB)(N_X/N_{In})]$ as a function of $1/T_{BLIP}$ because Eq. 5 can be rearranged to be

$$\frac{\alpha(\eta) N_V}{Q_B}\ \frac{N_X}{N_{In}} = \frac{\sigma_{In} g}{B}\ e^{E_X/kT_{BLIP}} \quad . \tag{6}$$

Note that Q_B is on the left hand side of the equation, in contrast to the arrangement in Ref. 2. This is to account for small variations in Q_B between samples. These quantities are shown plotted in Figure 3 along with the best-fitting line of the expected 0.111 eV slope. The large error bar shown for one point was due to uncertainty introduced by drift in that sample. The error bar is not typical of the other samples for which significantly smaller errors are estimated. The hatched area on the left side of the figure shows the range of value of T_{BLIP} found from Eq. 4 (that is, assuming that X has no effect for the samples plotted in the figure). The theoretical curve should make an asymptotic transition between the 0.111-eV line and the vertical hatched area (there is a family of transitions, slightly different for each sample). The lowest point shown in Figure 3 falls somewhat below the 0.111-eV line and probably lies on such a transition curve. T_{BLIP} for this sample is only 2.8° below the maximum possible value of T_{BLIP} calculated from Eq. 4 for this sample and background.

The data is in excellent agreement with the theoretical line, drawn for $B = 1.2 \times 10^{-6}$ cm^3/s. This value falls well within the range of values for B of 4×10^{-7} to 4×10^{-6} cm^3/s reported in the literature.[3]

The temperature dependence of D* for several Si:In detectors, both discrete and monolithic, is plotted in Figure 4. The data on the discrete detectors (the solid symbols) were all taken at the same bias and background conditions. Thus, the differences in the D* rolloff temperature, T_{BLIP}, are due to differences in the ratio of N_X to N_{In}, as discussed above. Sample C64701A was made from material grown in the large Czochralski furnace at Hughes Industrial Products Division (Carlsbad, California). This sample had a significantly lower X-level concentration than crystals grown in the smaller HRL furnaces. Also shown in the figure are data taken at several backgrounds from a monolithic discrete detector.

Theoretical curves are shown of D* for the no X-level case and for several N_X to N_{In} ratios. These curves were obtained by solving the T_{BLIP} equations given above as a function of Q_B, which was converted to D^*_{BLIP}. The right-most solid, no-X curve gives the optimum for Si:In photoconductive detectors. The dashed curves show the degradation resulting from various amounts of X. The dashed curves follow a 0.111-eV slope, and the solid curve follows 0.1572-eV slope. As the background is decreased, a given N_X/N_{In} imposes a relatively more severe penalty. Thus, while sample C64701A approaches pure In performance at $Q_B = 3 \times 10^{15}$, the small amount of X in the sample may still impose a 2° or 3° temperature penalty at $Q_B = 7 \times 10^{11}$. Of course, this represents a significant improvement over the previous high-X samples.

4. CARRIER LIFETIME

The carrier lifetime as a function of temperature and bias field was calculated from responsivity measurements. The usual equation for responsivity as a function of quantum efficiency and photoconductive gain can be rearranged to solve for lifetime:

$$\tau = \frac{Rh\nu}{e\eta} \frac{\ell^2}{\bar{\mu}V} , \qquad (7)$$

where R is the measured responsivity, $h\nu$ is the photon energy, e is the electronic charge, η is the quantum efficiency (which can be obtained either from D* measurements or from measurements of In concentration and absorption coefficient), ℓ is the sample thickness (electrical length), $\bar{\mu}$ is the

[2] R. Baron, M.H. Young, J.P. Baukus, O.J. Marsh, and J.J. Sheets, Proc. IRIS Det. Spec. Group Meet. (1977).

[3] A.G. Milnes, Deep Impurities in Semiconductors (John Wiley and Sons, New York, 1973), p. 290.

carrier mobility, and V is the bias voltage. In this case, η is calculated from:

$$\eta = \sigma_A N_{In} \ell \quad , \tag{8}$$

where σ_A is the absorption cross section, and N_{In} is the indium concentration measured by the Hall effect. The mobility used in Eq. 7 is calculated to include both the neutral scattering effects of the indium doping[4] and the high-yield velocity saturation effects as measured by Ottaviani et al.[5]

$$\bar{\mu} = \left(\frac{1}{\mu_{HALL}} + \frac{1}{\mu_{HOT}} \right)^{-1} \quad , \tag{9}$$

where μ_{HALL} is the value obtained from low-field Hall-effect measurements, and μ_{HOT}, the hot carrier mobility from Ref. 4, is a function of bias field, temperature, crystal orientation, and conductivity type.

The carrier lifetime is a function of the compensating dopant concentration and the recombination coefficient, B:

$$\tau = \frac{1}{B(N_D - N_B)} \quad . \tag{10}$$

Figure 5 is a plot of τ as obtained from responsivity measurements versus $(N_D - N_B)$ as measured by the Hall effect for several bias fields. The lines represent the least-squares fit of Eq. 10 to the data, and the resulting B values are indicated. The data represent samples grown by the float-zone and Czochralski techniques in both large and small furnaces. Also, the x and y values were obtained by completely independent measurements.

As the bias field is increased, the carrier lifetime increases. This is consistent with the Lax giant trap model,[6] which states that carrier recombination is through high excited states of the dopant. As the electric field is increased, lowering the barrier, holes in the excited states have an increasing probability of returning to the valence band and thus "live" longer as carriers. This barrier lowering is the Poole-Frenkle effect.[7]

These data were calculated from measurements taken at 40, 45, and 50 K for fields of approximately 200, 400, and 1800 V/cm. Fields varied from sample to sample by about 10%, which was not fully accounted for in the calculations. The values of B obtained by this procedure for these temperatures and fields are plotted in Figure 6 as a function of temperature. As temperature is increased, B becomes smaller (τ increases). This is because the larger values of kT encompass more and more excited states, which increases the probability for captured holes to return to the band. This effect is more fully discussed in another paper.[8] B also decreases with increasing electric field, as discussed above. The data show good correlation with both temperature and field, although more data over a wider range of the parameters are needed.

---

[4] R. Baron, M.H. Young, and T.C. McGill, Proc. 13th Int. Conf. Phys. Sem., Rome (1976).

[5] G. Ottaviani, L. Reggiani, C. Canali, F. Nava, and A. Alberigi-Quaranta, Phys. Rev. B12, 3318 (1975).

[6] M. Lax, J. Phys. Chem. Solids 8, 66 (1959).

[7] J.L. Hartke, J. Appl. Phsy. 39, 4871 (1968).

[8] R. Baron, M.H. Young, J.P. Baukus, and O.J. Marsh, Proc. IRIS Det. Spec. Group Meet. (1978).

The hole capture cross section, σ, can be calculated from the recombination coefficient:

$$B = \nu_{TH}\sigma \quad , \tag{11}$$

where B is the hole capture coefficient, and ν_{TH} is the thermal equilibrium carrier velocity:

$$\nu_{TH} = \left(\frac{8kT}{\pi m^*}\right)^{1/2} \quad , \tag{12}$$

where m* is the hole effective mass. Although some form of the conductivity effective mass would be more appropriate, the density of states effective mass is used because it is known.[9] The resulting discrepancy is not large.

The calculated capture cross section is plotted in Figure 7 as a function of temperature. Also plotted are the results of Norton et al.[10] on Si:P at lower temperatures and a range of values for Si:In at 77 K reported by Milnes.[3] Our data, which appear to be in quite good agreement with these values, provide information on the field dependence of the cross section. The agreement with the Si:P data is to be expected since the higher excited state spectra are similar for all dopants in silicon.

5. SUMMARY

We have measured the temperature and bias dependence of Si:In material from ingots that had been used to produce successful MFPAs. We found that the responsivity is directly proportional to the bias current for the usual fields and temperatures of MFPA operation. The responsivity becomes less temperature sensitive at higher fields and temperatures. The results of a refined calculation of the effect of the X level on detector performance were compared with experiment. The amount of X level in the present material causes a temperature penalty of only 2° to 3° at low backgrounds. We have also calculated the field and temperature dependence of the carrier recombination coefficient and cross section. To our knowledge, this is the first time that field-dependence data have been presented.

[9] H.D. Barber, Solid State Commun. 3, 299 (1965).

[10] P. Norton, T. Braggins, and H. Levenstein, Phys. Rev. Lett., 30, 488 (1973).

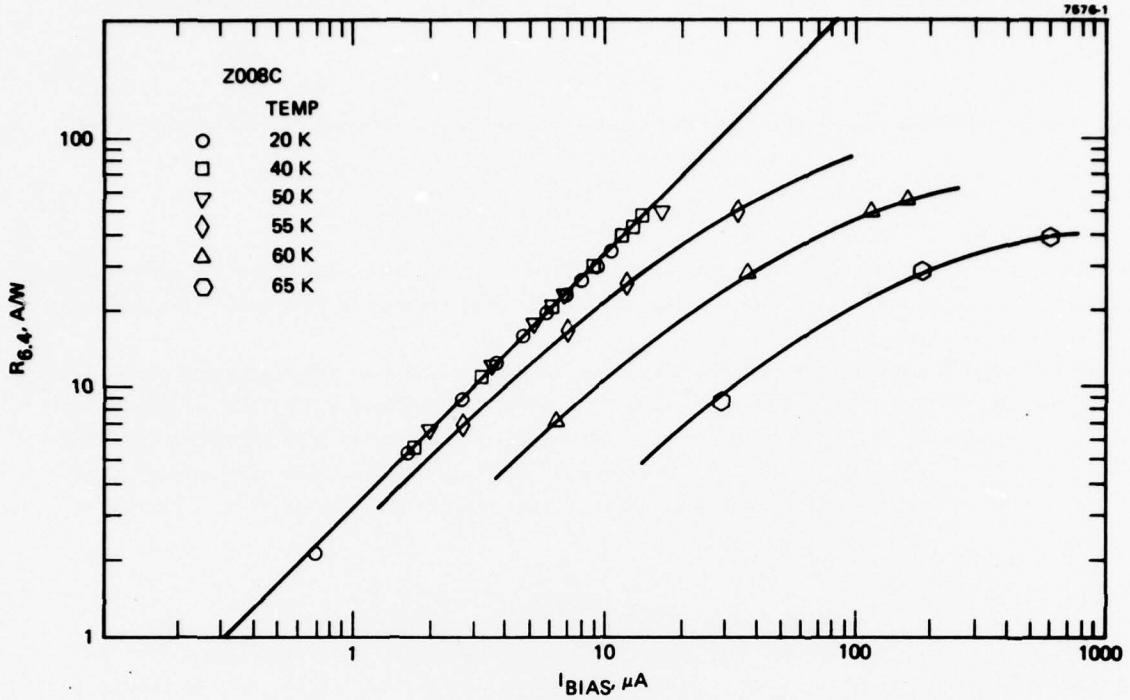

FIGURE 1. RESPONSIVITY VERSUS BIAS CURRENT. Responsivity of Si:In at 6.4 μm as a function of bias current. At high biases or temperatures the bias current increases more rapidly than the responsivity.

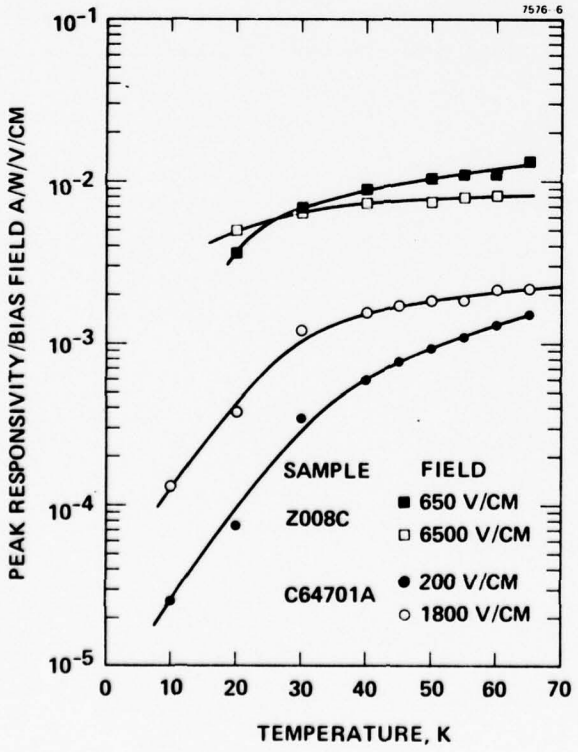

FIGURE 2. RESPONSIVITY VERSUS TEMPERATURE. Peak responsivity normalized to bias field plotted versus temperature for two Si:In samples. The responsivity becomes less sensitive to temperature as the bias is increased.

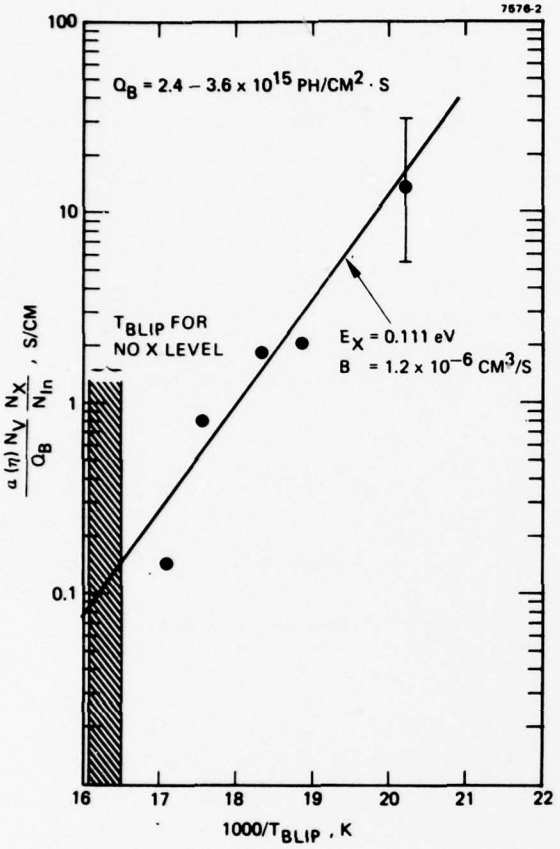

FIGURE 3. EFFECT OF X LEVEL ON T_{BLIP}. The effect of the N_X to N_{In} ratio on the D* rolloff temperature, T_{BLIP}, for several samples. The curve is a fit to the data using Eq. 6 with B as the fitting parameter. The shaded area on the left is the range of T_{BLIP} values that would be obtained if the samples had no X level.

7256-1

SYMBOL	TYPE	INGOT	N_{IN} · $\times 10^{17}$ CM^{-3}	N_X · $\times 10^{14}$ CM^{-3}	N_D · $\times 10^{14}$ CM^{-3}	N_X/N_{IN} $\times 10^{-3}$
△ ○ □	MONO	C20405	0.5	4	0.6	8
●	DISCRETE	C64701A	3.0	0.45	0.57	0.15
▲	DISCRETE	Z008A	1.7	1.8	0.08	1.1
■	DISCRETE	C21205T	2.2	19.0	1.1	8.6

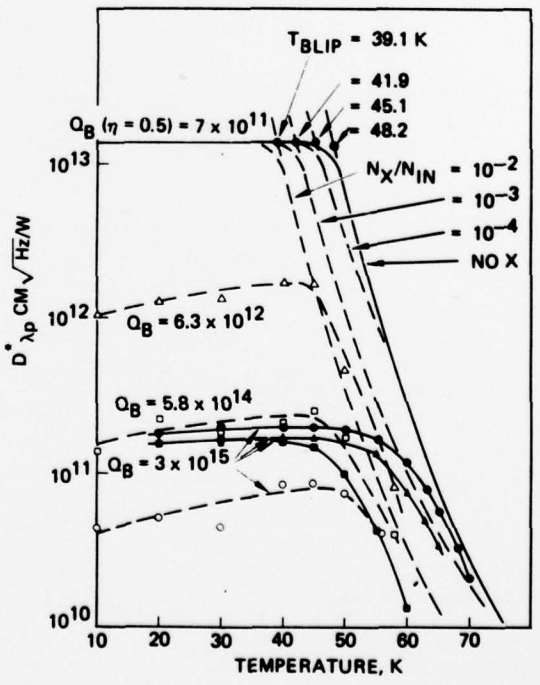

FIGURE 4. D* VERSUS TEMPERATURE. Peak D* versus temperature for Si:In discrete and monolithic discrete detectors. Also shown are theoretical curves for several N_X to N_{In} ratios. Photon background units are photons/sec-cm^2.

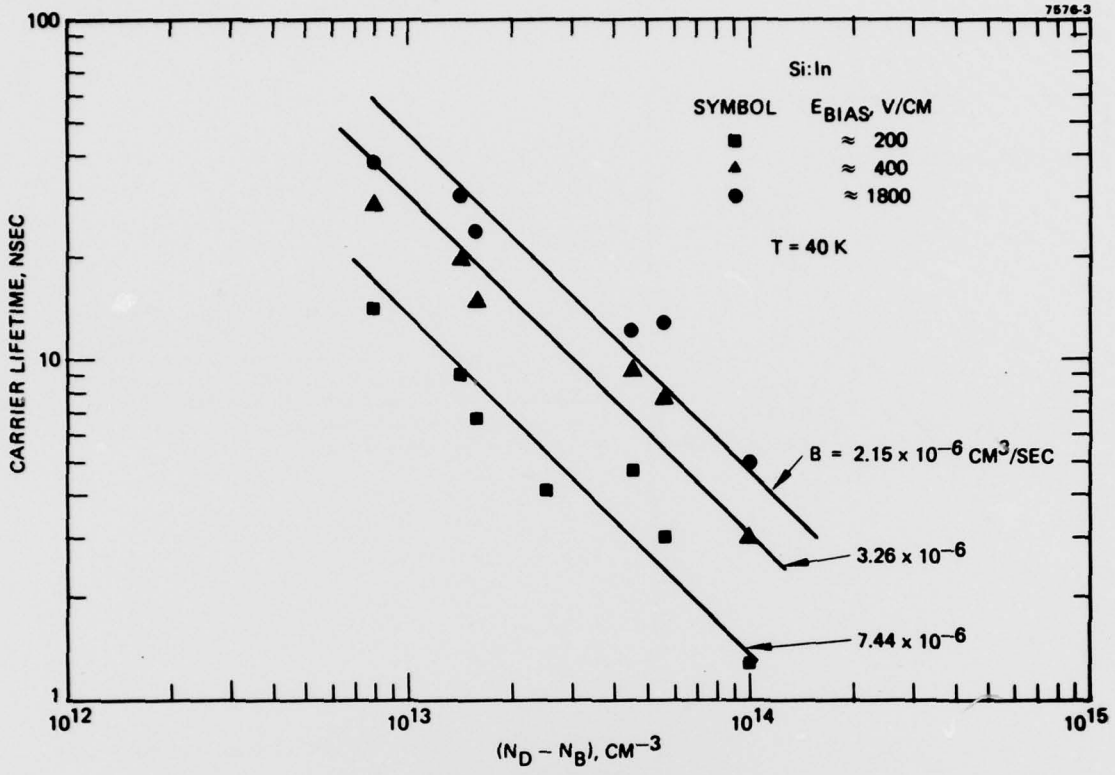

FIGURE 5. CARRIER LIFETIME VERSUS COMPENSATION. Carrier lifetime of Si:In at 40 K for three bias fields as a function of the net compensation concentration. The values of B were obtained from least-squares curve fits to Eq. 10.

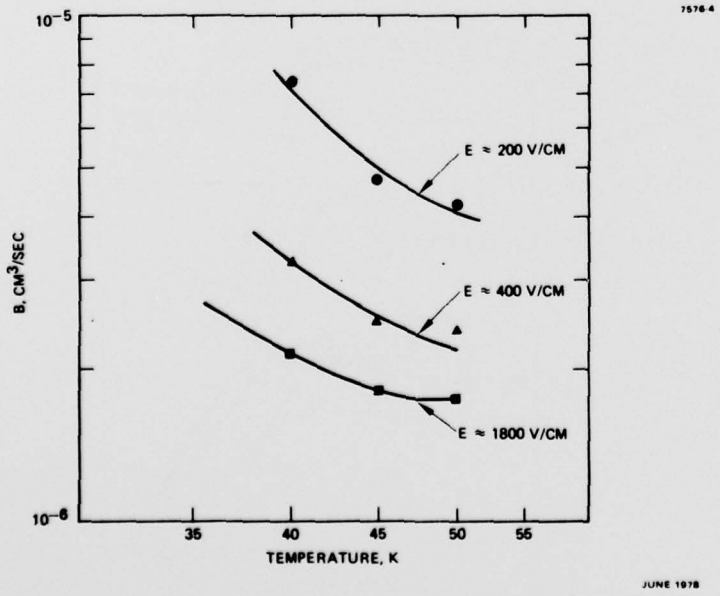

FIGURE 6. RECOMBINATION COEFFICIENT VERSUS TEMPERATURE. Plot of the recombination coefficient versus temperature for three bias fields.

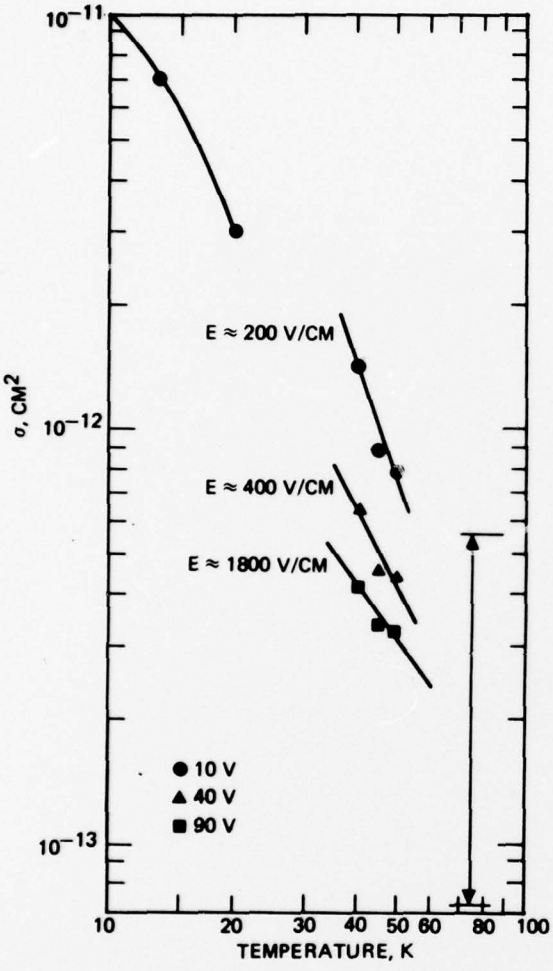

FIGURE 7. CAPTURE CROSS SECTION VERSUS TEMPERATURE. Hole capture cross section as a function of temperature for Si:In at three bias fields. The range of values indicated at 77 K are from Ref. 3. The values at 10 to 20 K are for Si:P and are from Ref. 10.

APPENDIX B

. . . . This paper is UNCLASSIFIED

UNCLASSIFIED

PHOTOLUMINESCENCE STUDIES OF ACCEPTORS IN SILICON*

S.A. Lyon, K.R. Elliott, G. Mitchard, D.L. Smith, and T.C. McGill

California Institute of Technology
Pasadena, California 91125

and

J.P. Baukus, R. Baron, M.H. Young, and O.J. Marsh

Hughes Research Laboratories
Malibu, California 90265

ABSTRACT

The photoluminescence spectra of doped Si are summarized, with particular emphasis on the spectra caused by the acceptors. The processes governing the relative intensity of the luminescence lines are discussed, and data is presented that makes it possible to estimate the relative intensity of the lines. New results are reported for the luminescence spectra of Si:In, including the observation of some unusually long-lived lines.

1. INTRODUCTION

Photoluminescence from excitons bound to impurity centers (BE) has been used as a diagnostic technique for several years. The primary emphasis of the work has been the III-V and II-VI semiconductors, which have potential as optoelectronic devices.[1] In the last few years a great deal of interest has developed in the luminescence spectra of silicon, both because it is an ideal system in which to study the fundamentals of the luminescence process[2-5] and because of potential for using the luminescence spectrum as a diagnostic measure of the impurity and defect concentration. This paper summarizes some of our recent results on the luminescence spectra of the acceptors in silicon with particular emphasis on Si:In.

Section 2 briefly describes the experimental technique. Section 3 presents some of the experimental data on the line positions for B, P, Al, Ga, In, and Tl, plus some of the complications of the spectra. Section 4 presents the data for two of the most important processes governing the photoluminescence process: the capture of an exciton on the impurity and the predominant decay mechanisms of the exciton once it is bound to the impurity. Section 5 presents the preliminary

*This research was supported by the Defense Advanced Research Projects Agency and monitored by the Army Night Vision Laboratory, under Contract No. DAAK70-77-C-0082.

[1] See, for example, A.A. Bergh and P.J. Dean, Light Emitting Diodes (Clarendeon Press, Oxford, 1976), and the references contained therein.

[2] S.A. Lyon, D.L. Smith, and T.C. McGill, Phys. Rev. B17, 2620 (1978).

[3] K.R. Elliott, G.C. Osbourn, D.L. Smith, and T.C. McGill, Phys. Rev. B17, 1808 (1978).

[4] S.A. Lyon, G.C. Osbourn, D.L. Smith, and T.C. McGill, Solid State Comm. 23, 425 (1977).

[5] K.R. Elliott, D.L. Smith, and T.C. McGill, Solid State Comm. 24, 461 (1978).

UNCLASSIFIED

results from a study of the luminescence from Si:In samples; we have observed several previously unknown lines, some with unusually long lifetimes. Section 4 summarizes our conclusions.

2. EXPERIMENTAL PROCEDURES

The experimental setup is shown in Figure 1. The Si samples were prepared by lapping and then etching with HNO_3:HF(7:1) and cleaning with methanol. The samples were then placed in a helium cryostat, and the bath temperature was measured using a Ge temperature sensor in the sample block. Electron-hole pairs were produced by irradiating the sample with above bandgap radiation from a GaAs or argon ion laser. The luminescence spectrum resulting from the recombination of an electron-hole pair bound to a neutral impurity was analyzed with a spectrometer, detected by a cooled S-1 photomultiplier, and processed using standard photon counting techniques. The type of signal observed is illustrated in the figure. It consists of a series of peaks of rather widely varying intensities.

3. LUMINESCENCE SPECTRA OF THE DOPANTS IN SILICON

The luminescence spectrum of a sample of Si:Al is shown in Figure 2. This data shows the spectrum in the region where the recombination occurs without a phonon, the no-phonon region. Other replicas of this spectrum are observed at energies corresponding to this spectrum except shifted by a phonon energy, the so called phonon-assisted transitions. The spectrum consists of several lines, some of them due to the Al dopant and others due to the background P impurity in the sample. All the lines labeled P are due to the impurity phosphorus. The line at approximately 1.1499 eV is due to the decay of a single electron-hole pair bound to P.[6] The other lines labeled P are due to the decay of a single electron-hole pair bound to a center with varying numbers of other electron-hole pairs bound to it. The lines labeled BE are due to the decay of a single electron-hole pair bound to a neutral Al. The other lines, labeled b_1, b_2, and b_3, are due to the decay of an electron-hole pair bound to a neutral center along with several other electron-hole pairs.[2]

This spectrum illustrates three important features. First, both donors and acceptors can be observed simultaneously in luminescence. Second, the lines for different impurities are displaced from each other in such a way that they can be resolved spectrally. Third, each impurity produces several lines, which give a unique signature for this impurity.

Figure 3 presents positions of the strongest line for each impurity, the so called principal bound exciton line. Again, this data illustrates the uniqueness of the spectral position of the line. Further, the energy positions of the lines for a given impurity are ordered according to the strength of the binding of the neutral impurity. This observation has been quantified to give the approximate Haynes rule.[7]

4. THE PHOTOLUMINESCENCE PROCESSES

To understand and quantify the observed photoluminescence spectrum requires an understanding of the various parts of the photoluminescence processes. To obtain information on the relative contributions of the various impurities, we need to understand the capture of the free exciton on the

---

[6] K. Kosai and M. Gershenzon, Phys. Rev. B9, 723 (1974).

[7] J.R. Haynes, Phys. Rev. Lett. 4, 361 (1960).

neutral impurity and the processes governing the relative strength of the various lines. The capture process is one in which a free exciton is captured by a neutral impurity, as characterized by a capture cross section. The measured capture cross section for Si:In is presented in Figure 4. The data shows that the capture cross section varies very rapidly with temperature: it is about 10^{-15} cm at 30 K and about 10^{-13} cm^2 at 10 K. The data shows a variation somewhat similar to that found for the capture of a carrier on an ionized center, where the mechanism is capture into highly excited states of the impurity center, the Lax giant trap mechanism.[8] Since we expect the highly excited states of the bound excitons to be very similar for different impurities, this cross section data should also apply to other impurities.

To estimate the relative strength of lines resulting from various impurities, we assume that the capture cross sections are the same for the impurities and that pump intensity is such that the lines are not saturated. That is, we assume that most of the impurity centers are not occupied by electron-hole pairs. With these reasonable assumptions, the relevant factors in the intensity, I, of a given line are given by

$$I \propto N \frac{R_R}{R_{NR} + R_R} \tag{1}$$

where N is the number of centers, and R_R and R_{NR} are the radiative and nonradiative rates, respectively. For Si, we can write

$$\frac{R_R}{R_{NR}} \leq 10^{-2} \quad .$$

This can be used to rewrite Eq. 1 as

$$I \propto N \frac{R_R}{R_{NR}} \quad . \tag{2}$$

The radiative rate is proportional to the oscillator strength, f, for a given transition:

$$R_R \propto f \quad . \tag{3}$$

In Figure 5, we have plotted the oscillator strength for the acceptors in the no-phonon transition. The data shows that oscillator strength increases with the binding of the acceptors according to the approximate relation

$$f \propto E_A^3 \quad . \tag{4}$$

where E_A is the binding energy of the hole on the acceptor. The predominant decay process for excitons on these impurities in Si is the nonradiative Auger process.[9] In this process, the electron-hole pair on the center recombines and the energy is carried away by the remaining carrier on the impurity center. The lifetime of the bound excitons on B, Al, and Ga due to this process is shown in Figure 6. Schmid[10] has made measurements of the lifetime for In, P, and A. He found

[8] M. Lax, Phys. Rev. 119, 1502 (1960).

[9] G.C. Osbourn and D.L. Smith, Phys. Rev. B16, 5426 (1977).

τ_{In} = 2.7 nsec, τ_p = 272 nsec, and τ_{As} = 183 nsec. The Auger decay rate increases rapidly with increasing binding energy.[9,10] This increase is given approximately by[9,10]

$$R_{NR} \propto E_A^n \tag{5}$$

where n is between 4 and 6.

Combining the results of Figures 5 and 6 or the approximate dependences given by Equations 4 and 5, we can obtain the correction relating the relative intensities to the relative number of centers. Using the approximate expression, the correction factor varies as E_A^{-m}, where m is in the range of 1 to 3. Thus, we find that the intensity for a given concentration decreases with increasing binding energy of the impurity but not as fast as the Auger rate would suggest.

5. PHOTOLUMINESCENCE SPECTRA OF Si:In SAMPLES

The interest in Si:In for making infrared detectors and the need to understand the origin of the "x-level"[11] has led to a study of the luminescence of Si:In samples. In Figure 7 is the luminescence spectrum of one of the Si:In samples. The spectrum is dominated by several very intense lines (labeled BE) that are due to the In dopant. Other lines (labeled A, B, and C) are intense and of unknown origin. They have not been observed in samples doped with Ga or Al or any of the donors. These lines tend to be much stronger in Czochralski-grown material as compared to samples prepared by the float zone technique. At one point, these lines were thought to be likely candidates for the "x-level" (see the discussion of the transients below). Several other lines of unknown origin are also indicated in the spectrum (by question marks). The positions of all of the lines and their assignments are, where possible, given in Table 1.

The lines labeled A, B, and C were investigated by studying their sample dependence, decay characteristic, and temperature dependence. The most unusual property of each line is its decay characteristic. Figure 8 shows the decay characteristics of the A and C lines. The measured decays are exponential and yield decay times on the order of a few hundred microseconds. These decay times are unusually long for excitons in Si. All of the other decay times measured for bound excitons in Si are typically less than a few microseconds. Hence, these lines possess decay times that are at least two orders of magnitude larger than other lines observed in Si. Very recently, Weber, Schmid, and Sauer[12] observed lines with different energies than those reported here but with very long decay times. They interpret these lines as resulting from isoelectronic traps associated with carbon in Si. It seems very likely that the lines we have observed are due to an isolectronic center in the Si and that the observed decay time is the radiative decay time for the center. Since these lines have only been observed in samples doped with In, it seems likely that they involve In.

We are presently studying the other lines in the Si:In spectrum and hope to report on them shortly.

[10] W. Schmid, Phys. Stat. Solidi b84, 529, (1977).

[11] R. Baron, M.H. Young, J.K. Neeland, and O.J. Marsh, Appl. Phys. Lett. 30, 594 (1977).

[12] J. Weber, W. Schmid, and R. Sauer, private communication.

6. SUMMARY

We have given a brief summary of some of our results on the photoluminescence spectra of acceptors in Si. The results show that the photoluminescence lines for an impurity give a unique signature for that impurity and that we should be able to use this technique as a diagnostic tool for looking at the impurities in infrared detector materials. We presented the results for the parameters that would allow us to convert relative line intensity data to relative concentrations.

Finally, we presented some new results on the Si:In luminescence that suggest that In forms a center in Si that acts as an isoelectronic trap. Several new lines were reported for the Si:In samples.

Table 1. The energy and assignment of some of the lines observed in the photoluminescence spectrum shown in Figure 7 for a Si:In sample

Peak Energy,[a] MeV	Identification
1077.6	?
1082.0	TO + LO phonon In BE (J = 0)
1085.1	TO + LO phonon In BE (J = 2)
1093.3	?
1098.4	TO + LO phonon FE
1101.1	?
1105.7	?
1108.6	A
1110.7	?
1114.4	?
1115.9	B
1117.7	C
1121.5	TA phonon In BE (J = 0)
1125.0	TA phonon In BE (J = 2)
1129.2	?
1136.5	?
1140.5	In BE (J = 0)
1143.7	In BE (J = 2)
1154.3	?

[a]Energies accurate to about ±0.2 meV.

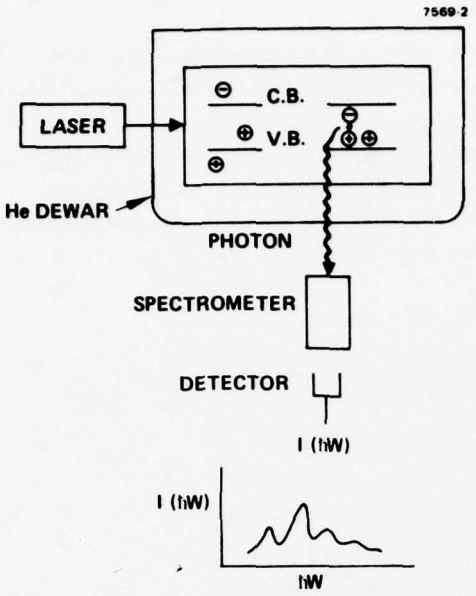

Figure 1.
Schematic of the experimental setup and the photoluminescence process.

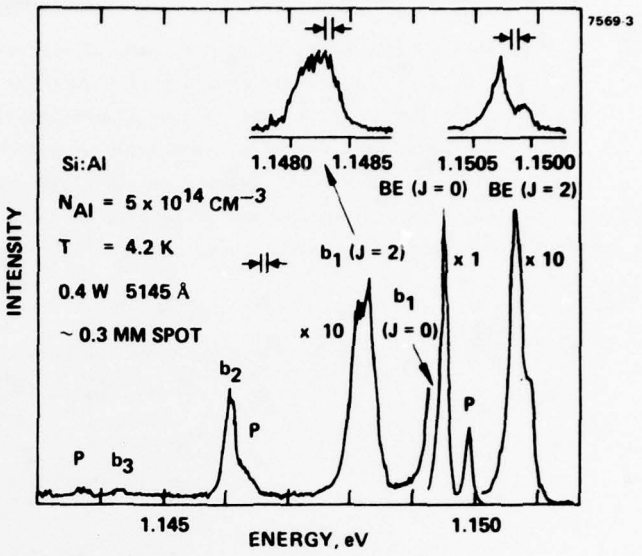

Figure 2.
The photoluminescence spectra of Al doped Si in the energy range for no-phonon assisted transitions. The lines labeled BE, b_1, b_2, and b_3 are associated with Al impurities. The lines labeled P are associated with phosphorous impurities in the Si.

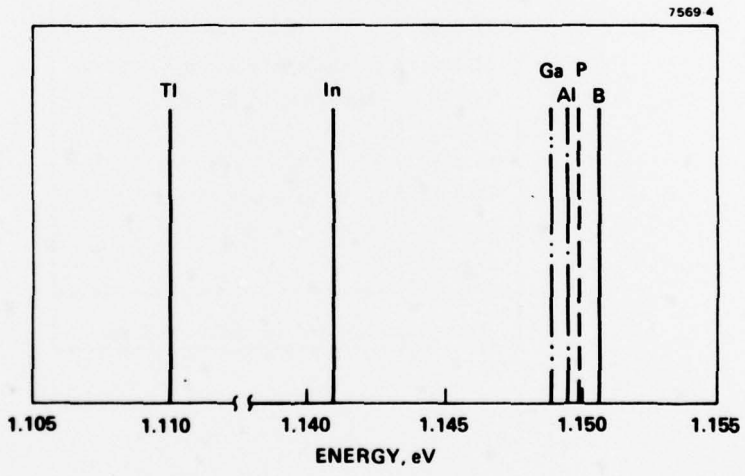

Figure 3.
The position of the principal bound exciton line for various impurities in the no-phonon assisted transition. The positions for B and P were taken from Ref. 6.

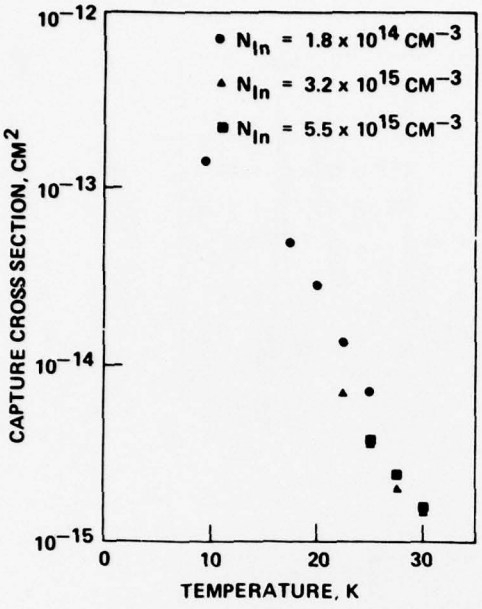

Figure 4.
The measured temperature dependence of the capture cross section of free excitons on neutral indium impurities in silicon. The data is given for different doping levels ranging from 1.8 x 10^{14} to 5.5 x 10^{14} cm^{-3}.

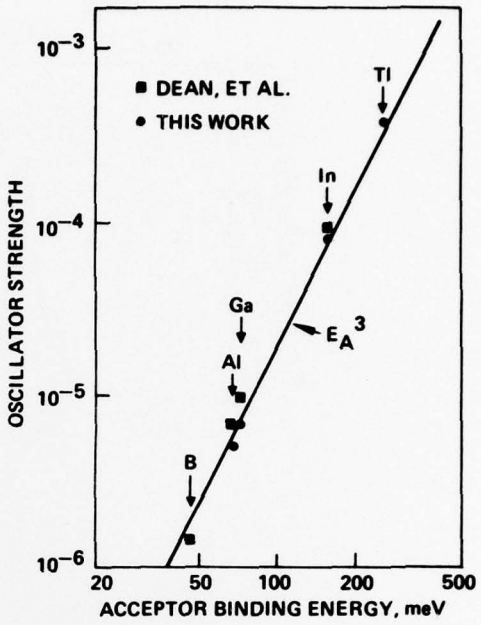

Figure 5.
The total absolute oscillator strength for the lowest known transitions of an electron-hole pair bound to an acceptor. The data indicated by ■ were taken from P.J. Dean, W.F. Flood, and G. Kaminsky (Phys. Rev. 163, 721 (1967))

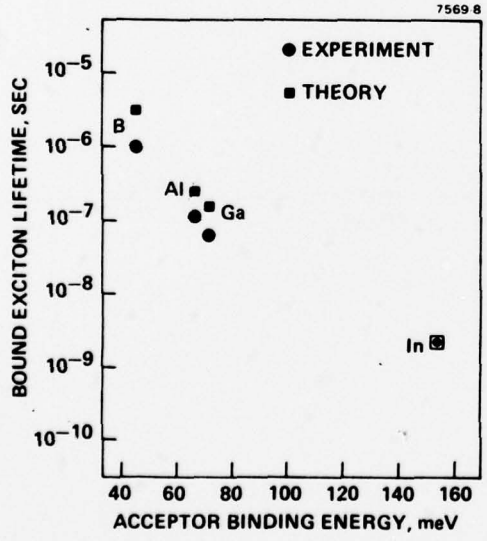

Figure 6.
Bound exciton lifetimes versus impurity binding energy for the four common acceptors in Si. The solid circles are measured values and the squares are calculations of the Auger lifetime. The measured value for Si:In is from Ref. 10.

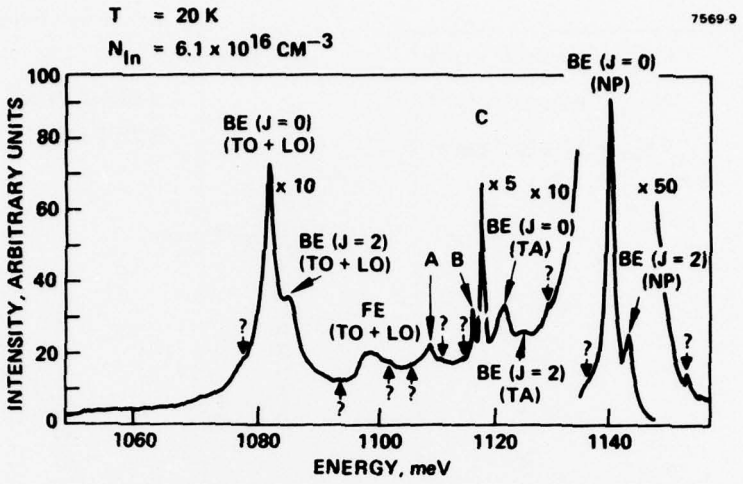

Figure 7.
The luminescence from a Czochralski-grown Si:In sample. The lines labeled BE are due to an electron-hole pair bound to a neutral In. The lines labeled with A, B, C, and the lines labeled with ? are of unknown origin.

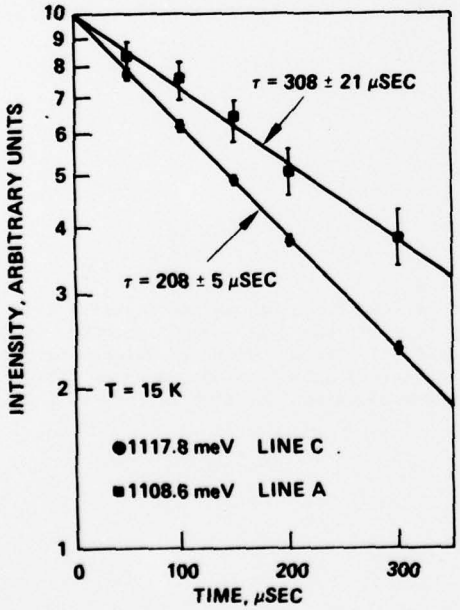

Figure 8.
The decay characteristics of the lines labeled A and C in Figure 7.

DISTRIBUTION LIST FOR FINAL TECHNICAL REPORTS
(1 Copy Unless Otherwise Specified)
Semi-Annual Plus Final Reports

Defense Documentation Center
ATTN: DDC-TCA
Cameron Station, Bldg 5
Alexandria, VA 22314
(12 copies)

Director
National Security Agency
ATTN: TDL
Fort George G. Mead, MD 20755

Office of Naval Research
Code 417
Arlington, VA 22217

Director
Naval Research Laboratory
ATTN: Code 2627
Washington, D.C. 20375

Commander
Naval Electronics Laboratory Center
ATTN: Library
San Diego, CA 92152

Commander
US Naval Surface Weapons Laboratory
ATTN: Dr. F. Bis
White Oak, Silver Spring, MD 20910

Commandant
Marine Corps
HQ, US Marine Corps
ATTN: Code LMC
Washington, D.C. 20380

Air Force Avionics Laboratory
ATTN: AFAL/TSR, STINFO
Wright-Patterson Air Force Base,
Ohio 45433

OSASS-RD
Washington, D.C. 20310

CDR, US Army Materiel Command
ATTN: AMCMA-EE
5001 Eisenhower Avenue
Alexandria, VA 22333

CDR, US Army Materiel Command
ATTN: AMCRD-FW
5001 Eisenhower Avenue
Alexandria, VA 22333

Commander
US Army Missile Command
ATTN: AMSMI-RR,
Dr. J.P. Hallowes
Redstone Arsenal, AL 35809

Commander
US Army Armament Command
ATTN: AMSAR-RDP (Library)
Rock Island, IL 61201

Commander
Picatinny Arsenal
ATTN: SARPA-TS-S $59
Dover, NJ 07801

Commander
USASA Test & Evaluation Center
Fort Huachuca, AZ 85613

US Army Research Office-Durham
ATTN: CRDARD-IP
Box CM, Duke Station
Durham, NC 27706

US Army Research Office-Durham
ATTN: Dr. Robert J. Lontz
Box CM, Duke Station
Durham, NC 27706

HQDA (DACE-CMS)
Washington, D.C. 20310

Aerojet
Electro System Company
ATTN: P.C. Wang
1100 W. Hollyvale Street
Azusa, CA 91702

Arthur D. Little Incorporated
Acron Park
ATTN: Jacques M. Steininger
Cambridge, MA 02140

Barnes Engineering
ATTN: Dr. W. Rolls
30 Commerce Road
Stamford, CT 06902

Battelle Memorial Institute
Library
505 King Avenue
Columbus, OH 43201

Cincinnati Electronics Corporation
ATTN: Dr. Vernon Lambert
2630 Glendale-Milford Road
Cincinnati, OH 45241

Electro-Optical Systems, Inc.
Solid State Department
ATTN: Dr. P.J.A. Zoutendyk
300 N. Halstead Street
Pasadena, CA 91107

Fairchild Company
Charge Coupled Device Department
ATTN: Dr. R.H. Dyck
Palo Alto, CA 94304

Ford Motor Company
Scientific Research Staff
ATTN: Dr. H. Holloway
P.O. Box 2053
Dearborn, MI 48121

General Dynamics
ATTN: Dr. Ester Krikorian
Mission Blvd.
Pomona, CA 91766

Honeywell Inc.
Aerospace & Defense Group
Infrared Detector Group
ATTN: George D. Anderson
1611 North Kent Street
Arlington, VA 22209

Hughes Research Laboratories
ATTN: Lloyd DeVaux
3011 Malibu Canyon Road
Malibu, CA 90265

RCA Laboratories
ATTN: R.L. Foley
Princeton, NJ 08540

Lincoln Laboratory
Massachusetts Institute of Tech.
ATTN: Dr. I. Melngailis
Lexington, MA 02173

Perkin-Elmer Corporation
Associate Director of Research
ATTN: Dr. David A. Huchital
Norwalk, CT 06852

Aeronutronics Ford Corporation
Fort Road
ATTN: Mr. Sutton
Newport Beach, CA 92663

Rockwell International Corporation
Autonetics Division
ATTN: Dr. G. Hoover or
Dr. R.C. Geiss
P.O. Box 4192
3370 Miraloma Avenue
Anaheim, CA 92803

Rockwell International Corporation
Science Center
ATTN: Library (H.M. Coogan)
1049 Camino Dos Rios
Thousand Oaks, CA 91360

Commander
HQ MASSTER
Technical Information Center
ATTN: Mrs. Ruth Reynolds
Fort Hood, TX 76544

USA Security Agency
ATTN: IARD
Arlington Hall Station
Arlington, VA 22212

Commander
US Army Missile Command
ATTN: AMSMI-RE (Mr. Pittman)
Redstone Arsenal, AL 35809

Commander
US Army Systems Analysis Agency
ATTN: (Mr. A. Reid),
AMXSY-T
Aberdeen Proving Ground, MD 21005

NASA Scientific & Tech Info
Facility
ATTN: Acquisitions Branch
(S-AK/DL)
PO Box 8757
Baltimore-Washington
International Airport
Baltimore, MD 21240

Chief
Ofc of Missile Electronic Warfare
Electronic Warfare Lab, ECOM
White Sands Missile Range,
NM 88002

Director
Defense Advanced Research
Projects Agency
1400 Wilson Blvd.
ATTN: Dr. R. Reynolds
Arlington, VA 22209
(3 cys)

Naval Postgraduate School
ATTN: Dr. F. Tao (52-TV)
Monterey, CA 93940

USNADC
ATTN: Dr. M. Hess
Code 202149
Warminster, PA 18974

Institute for Defense Analyses
ATTN: Dr. A.D. Schnitzler
400 Army-Navy Drive
Arlington, VA 22202

Infrared Information and
Analysis Center
PO Box 618
Ann Arbor, MI 48107

Advisory Group on Electron Devices
201 Varick Street, 9th Floor
New York, NY 10014

Commander
US Army Electronics Command
ATTN: DRSEL-MS-TI
Fort Monmouth, NJ 07703

Commander
US Army Electronics Command
ATTN: DRSEL-PL-ST
Fort Monmouth, NJ 07703